# TOWARDS INTERPRETABLE PROTEIN STRUCTURE PREDICTION WITH SPARSE AUTOENCODERS

**Anonymous authors**
Paper under double-blind review

## ABSTRACT

Protein language models have revolutionized structure prediction, but their nonlinear nature obscures how sequence representations inform structure prediction. While sparse autoencoders (SAEs) offer a path to interpretability here by learning linear representations in high-dimensional space, their application has been limited to smaller protein language models unable to perform structure prediction. In this work, we make two key advances: (1) we scale SAEs to ESM2-3B, the base model for ESMFold, enabling mechanistic interpretability of protein structure prediction for the first time, and (2) we adapt Matryoshka SAEs for protein language models, which learn hierarchically organized features by forcing nested groups of latents to reconstruct inputs independently. We demonstrate that our Matryoshka SAEs achieve comparable or better performance than standard architectures. Through comprehensive evaluations, we show that SAEs trained on ESM2-3B significantly outperform those trained on smaller models for both biological concept discovery and contact map prediction. Finally, we present an initial case study demonstrating how our approach enables targeted steering of ESMFold predictions, increasing structure solvent accessibility while fixing the input sequence. Upon publication, we plan to release our code, trained models, and visualization tools to facilitate further investigation by the research community.

## 1 INTRODUCTION

Machine learning-based protein structure prediction models have achieved remarkable success by leveraging vast amounts of sequence data (Jumper et al., 2021; Lin et al., 2022), building on the success of previous sequence homology-based methods (Marks et al., 2011; Kamisetty et al., 2013). However, their nonlinear nature prevent easily understanding how sequence information informs structure prediction compared to previous statistical methods with simple linear priors.

Previous interpretability studies on transformer-based protein language models (PLMs) have demonstrated PLMs, despite only training on sequences, learn structural information. Rao et al. (2021) and Vig et al. (2021) showed that the attention map learns to predict residue-residue contacts. Zhang et al. (2024) show PLMs predict structure primarily by memorizing and retrieving patterns of coevolving residues rather than learning fundamental biophysical principles. However, these works are limited to correlational analyses between model behaviors and biological patterns, failing to establish causal relationships between internal mechanisms and predictions.

Mechanistic interpretability through sparse autoencoders (SAEs) offers a promising direction for understanding these black box models by learning interpretable linear representations (Templeton et al., 2024; Gao et al., 2024), similar to how earlier statistical methods successfully used linear priors to capture sequence-structure relationships. While modern PLMs achieve superior performance through complex nonlinear transformations, SAEs can potentially bridge this interpretability gap by decomposing these transformations into human interpretable features in a linear high-dimensional latent space.

SAEs have previously been trained on protein language models in the ESM2 series (Simon and Zou, 2024; Adams et al., 2025), identifying thousands of features which correspond to manually-annotated biological concepts and functional properties. However, the subject PLMs used in previ-

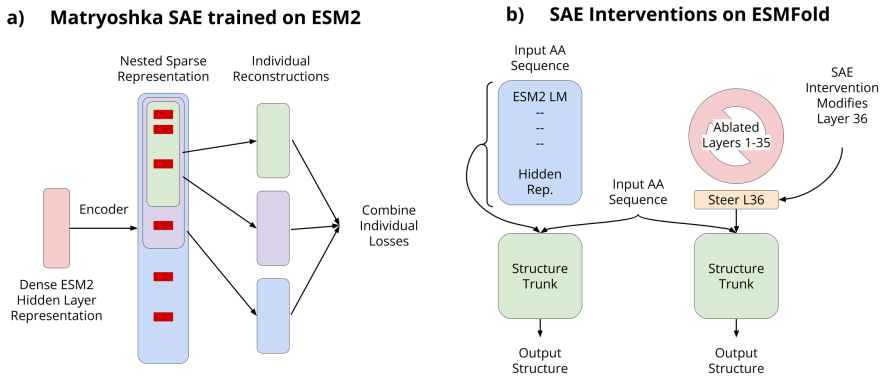


Figure 1: a) Matryoshka Sparse Autoencoder (SAE) architecture for training on ESM2 hidden layer representations, showing nested sparse feature organization. b) SAE intervention framework for ESMFold, comparing normal operation (left) where all ESM2 hidden representations flow to the structure trunk, versus intervention (right) where only a modified layer 36 representation is used while ablating all other layers.

ous works were too small to enable interpretability on ESMFold, the structure prediction head on top of ESM2.

Our work advances protein model interpretability in two key directions. First, we scale SAEs to ESM2-3B, the base model for ESMFold, enabling mechanistic interpretability of protein structure prediction for the first time. Second, we adapt Matryoshka SAEs (Nabeshima, 2024; Bussmann et al., 2024) to PLMs, which learn features at multiple scales of detail. This hierarchical organization not only aligns with the multi-scale nature of protein structure but also improves feature disentanglement and interpretability compared to standard sparse autoencoders.

We structure the paper as follows:

1. In Section 2, we present our methodological advances: scaling SAEs to ESM2-3B and adapting Matryoshka SAEs, a recently developed SAE architecture that learns hierarchically organized features.
2. In Section 3, we validate our approach by demonstrating Matryoshka SAEs achieve comparable or better performance than L1 and TopK architectures on both language modeling and structure prediction tasks.
3. In Section 4, we show the benefits of interpreting larger PLMs through ESM2-3B's superior performance on biological concept discovery and contact map prediction tasks.
4. In Section 5, we demonstrate practical applications through an initial steering case study, showing how we can increase the solvent accessibility of a predicted structure while fixing the input sequence.
5. In Appendix A, we include a "meaningfulness statement" describing what we think constitutes a meaningful representation of life and how this work contributes to this direction.

To enable the community to extend our work and continue investigating, we will release our code and trained models open-source accompanied by a visualizer upon publication.

## 2 METHODS

### 2.1 SETUP

**Problem Statement.** For each token of a protein sequence, a transformer encoder-based PLM outputs an embedding $x \in \mathbb{R}^d$ in each layer $\ell$. A sparse autoencoder encodes the embedding $x$ to a higher-dimensional latent representation $z \in \mathbb{R}^n$ where $d << n$ and decodes it as $\hat{x}$. The

SAE is trained by minimizing the L2 reconstruction loss between the original embedding $x$ and its reconstruction $\hat{x}$, defined as $\mathcal{L} = \|x - \hat{x}\|_2^2$.

To learn meaningful representations, sparsity constraints are imposed on the latent vector $z$. This sparsity can be achieved either through L1 regularization terms in the loss function or through specialized activation functions that directly restrict the number of non-zero elements. In practice, the number of active (non-zero) elements $K$ satisfies $K \ll d \ll n$, preventing degenerate solutions such as the identity map.

**Subject Models.** We train SAEs on the ESM2 series of PLMs (Lin et al., 2022). We focus primarily on the 3 billion parameter model ESM2-3B which provides representations for ESMFold.

**Hyperparameters.** We train SAEs on layer 18 and 36 of ESM2-3B, the middle and last layer respectively. During training, we normalize our embeddings to have average unit L2 norm enabling hyperparameter transfer between layers. During inference, we unnormalize by scaling the biases following Marks et al. (2024).

**Data.** We randomly selected 10M sequences from Uniref50, the training set of ESM2, constituting 2.5 billion tokens. See Appendix G.2 for details.

### 2.2 MATRYOSHKA SAEs

**Background.** Biological systems inherently exhibit hierarchical organization, from atomic interactions to molecular assemblies to cellular structures to entire organisms. This hierarchical nature is reflected in protein sequences, where information is encoded at multiple scales - from local amino acid patterns to higher-order structural motifs. To capture these multi-scale features, we employ Matryoshka Sparse Autoencoders (SAEs), which learn nested hierarchical representations of protein sequence embeddings (Nabeshima, 2024; Bussmann et al., 2024). Like their namesake Russian dolls, these autoencoders embed lower-dimensional representations within higher-dimensional ones, allowing simultaneous optimization of features at multiple scales. For a visual diagram, see Fig. 1a.

**Architecture.** The Matryoshka SAE architecture divides its latent dictionary into nested groups of increasing size, with each group building upon the previous ones. When processing a protein token embedding $x \in \mathbb{R}^d$ from a PLM, each group must learn to reconstruct the input using only its allocated subset of latents. This progressive constraint naturally encourages the emergence of a feature hierarchy - earlier groups must capture high-level, abstract features to achieve reasonable reconstruction with limited capacity, while later groups can encode more granular details.

**Encoding.** We follow Bussmann et al. (2024) and Marks et al. (2024) where given an token embedding $x \in \mathbb{R}^d$, the encoding process follows as

$$z = \text{BatchTopK}(W_{\text{enc}} x + b_{\text{enc}}) \tag{1}$$

where $W_{\text{enc}} \in \mathbb{R}^{n \times d}$ is the encoder weight matrix, $b_{\text{enc}} \in \mathbb{R}^n$ is the encoder bias, and BatchTopK enforces sparsity by keeping only the $B * K$ highest activations in each batch. This enforces average sparsity while allowing the number of active latents per token to vary.

**Decoding and Loss.** The key innovation of Matryoshka SAEs lies in their group-wise decoding process:

$$\hat{x}^{(m)} = W_{\text{dec}}^{(m)} z_{[1:m]} + b_{\text{dec}} \tag{2}$$

Here, $z_{[1:m]}$ represents the first $m$ components of the latent vector, $W_{\text{dec}}^{(m)} \in \mathbb{R}^{d \times m}$ is the decoder weight matrix restricted to its first $m$ columns, and $b_{\text{dec}} \in \mathbb{R}^d$ is the decoder bias. Each group $m$ must reconstruct the input using only its allocated subset of latents. The total loss combines reconstruction errors across all group sizes $M$:

$$\mathcal{L}(x) = \sum_{m \in M} \|x - \hat{x}^{(m)}\|_2^2 + \alpha \mathcal{L}_{\text{aux}} \tag{3}$$

where $\alpha$ weights any auxiliary regularization terms. We use the auxiliary loss term from Marks et al. (2024) and Gao et al. (2024) to reduce dead latents.

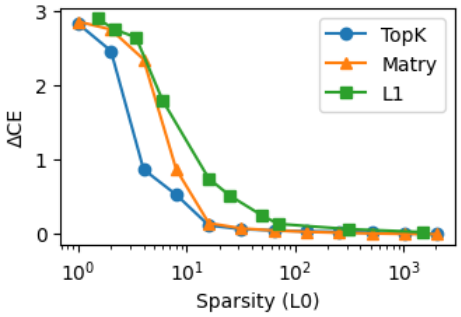


(a) CE loss reconstruction across sparsity levels for TopK, Matryoshka (Matry), and L1 regularized autoencoders. Matryoshka requires similar or less active latents to achieve good reconstruction.

| Comparison | RMSD (Å) |
|---|---|
| Exp vs. ESMFold (baseline) | 3.1 ± 2.5 |
| Exp vs. ESMFold (full ablation) | 15.1 ± 5.9 |
| Exp vs. ESMFold (only layer 36) | 2.9 ± 2.1 |
| Exp vs. SAE (layer 36) | 3.2 ± 2.6 |
| ESMFold vs. SAE (both L36) | 3.1 ± 4.4 |

(b) Backbone RMSD (Å) comparing experimental structures (Exp), ESMFold predictions, and SAE reconstructions. Keeping layer 36 or using SAE preserves accuracy, while full ablation degrades performance.

Figure 2: Downstream loss evalautions on a) language modeling and b) structure prediction.

## 3 Evaluations on Downstream Loss

We evaluate our SAEs on language modeling and structure prediction for ESM2-3B and ESMFold respectively to assess how well they preserve performance on downstream tasks.

### 3.1 Language Modeling

**Setup.** We report the average difference in cross-entropy loss $\Delta CE$ between the logits from the original and SAE reconstructed PLM. We evaluate on 1024 random sequences in CATH (Sillitoe et al., 2020) following Simon and Zou (2024) on layer 36 of ESM2. [1]

**Results.** Figure 2a shows the impact of different autoencoder architectures on downstream language modeling performance across sparsity levels. For architecture details, see Appendix G.1. At low sparsity ($L_0 < 10$), all approaches - TopK, Matryoshka, and L1 regularization - show similar degradation ($\Delta$CE $\approx$ 2.5–3.0). As sparsity increases, TopK and Matryoshka SAEs maintain better performance compared to L1 regularization, with $\Delta$CE approaching 0 for sparsity levels above 100.

### 3.2 Structure Prediction

**Setup.** By scaling SAEs to ESM2-3B, we can now evaluate how well our SAE representations preserve ESMFold's structure prediction capabilities. We focus on reconstructing ESM2's hidden representations that feed into ESMFold. Since ESMFold uses representations from all layers but our SAE reconstructs only one layer, we ablate all other layers to isolate reconstruction effects. This ablation maintains performance on the CASP14 test set (see Fig. 2b).

**Data.** We evaluate structure prediction on the CASP14 dataset, a diverse challenging dataset that is held out from ESMFold during training. We filter out sequences that 1) are longer than 700 residues so that our evaluations can fit on one GPU and 2) have ESMFold predictions with RMSD $>$ 10 Å compared to the experimental structure, leaving 17 / 34 targets. Full list in Appendix D.

**Results.** Our experiments demonstrate effective preservation of structural information. In Fig. 2b, we see that comparing experimental structures to ESMFold predictions shows an RMSD of 3.1 ± 2.5 Å without ablation. While full ablation of ESM2 embeddings significantly degrades performance (RMSD 15.1 ± 5.9 Å), both keeping only layer 36 (RMSD 2.9 ± 2.1 Å) and using our SAE reconstruction (RMSD 3.2 ± 2.6 Å) maintain comparable performance. The similarity between ESMFold and SAE predictions (RMSD 3.1 ± 4.4 Å) confirms preservation of structural information.

[1] Results on a held-out Uniref50 test set and layer 18 will be included in the final version.

These results show our SAE effectively compresses model representations while maintaining both sequence-level and structural prediction capabilities across sparsity levels.

# 4 Further Evaluations

## 4.1 Swiss-Prot Concept Discovery

We evaluate feature interpretability through alignment with Swiss-Prot annotations, following the methodology of Simon and Zou (2024) with background in Appendix Section C.1. Our evaluation encompasses 476 biological concepts (256 domains, 98 residue-level features, 55 regions, 37 motifs, 15 zinc fingers, 5 targeting peptides, and 10 other features), analyzing 30,871,402 amino acid tokens (approximately 21% of Swiss-Prot) (Table 1).

**Methodology.** Concepts are included if they contain either more than 1,500 total amino acids or appear in more than 10 domains within our dataset. Features are considered to capture a concept if they achieve an F1 score above 0.5, calculated using the modified domain-level recall metric in Simon and Zou (2024) that accounts for varying granularity between feature activations and concept annotations. For consistent evaluation across architectural variants, we perform post-hoc normalization by scaling feature activations to [0,1] based on maximum activation values across the evaluation set.

**Results.** When comparing models trained on ESM2-3B versus ESM2-8M (both using dictionary size 20,480 and sparsity k=100), we find SAEs trained on ESM2-3B capture substantially more biological concepts with higher F1 scores achieved for each concept (Figure 5). The 3B Matryoshka model generates 2,677 high-quality feature-concept pairs of F1 $>$ 0.5, compared to 287 pairs for its 8M counterpart, while the TopK variants produce 2,461 and 844 pairs respectively (Figure 3a).

Both 3B variants identify 233 distinct concepts (48.9% of total) with F1 scores above 0.5, compared to 72 (15.1%) and 95 (20.0%) concepts for the 8M Matryoshka and TopK variants (Table 1). This improved coverage spans all categories, with particularly strong performance in protein domains where 3B models capture 76% of concepts versus 19.5-28.1% in 8M models. Head-to-head comparison shows 3B models achieve higher F1 scores on over 400 concepts, with an average improvement of 0.25, while architectural variants at the same scale show minimal differences (Figure 6). See Appendix Section C.2 for additional details on model performance.

## 4.2 Contact Map Prediction

**Background.** Following Zhang et al. (2024), we evaluate our SAEs' ability to capture coevolutionary statistics through contact map prediction using the Categorical Jacobian. Details in Appendix E. This provides an unsupervised test of whether our compressed representations preserve the structural information encoded in the original model.

**Results.** We assess contact prediction accuracy using the precision at L/2 metric (P @ L/2), which measures the fraction of correctly predicted contacts among the top L/2 predicted long-range contacts, where L is the protein sequence length. Figure 3b shows the correlation between contact prediction accuracy of ESM2 and our SAE reconstructions across different model scales. The 3B model demonstrates consistently higher precision compared to the 8M model, with reconstructions closely tracking the original ESM2 predictions. [2] This suggests that larger language models capture more robust coevolutionary signals that can be effectively compressed by our approach.

# 5 Case Study: SAE Feature Steering on ESMFold

## 5.1 SAEs on ESMFold Help Identify Structural Features

Building on previous work by Simon and Zou (2024), we investigated whether targeted feature manipulation of ESM2-3B could induce coordinated changes in both sequence composition and predicted structure through ESMFold's pipeline. Using our Matryoshka SAE trained on ESM2-3B, we identified a feature strongly correlated with residue hydrophobicity. Following the feature

[2] The current version of these results are biased and will be corrected. See Appendix E.

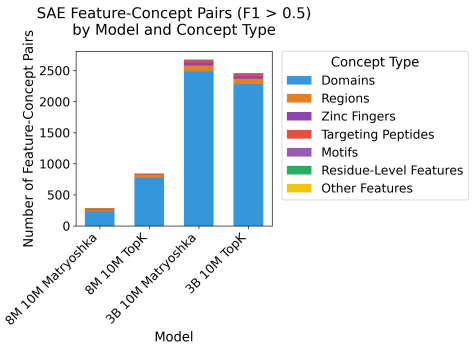


(a) Number of high-performing feature-concept pairs (F1 $>$ 0.5) across model scales and architectures, broken down by concept type.

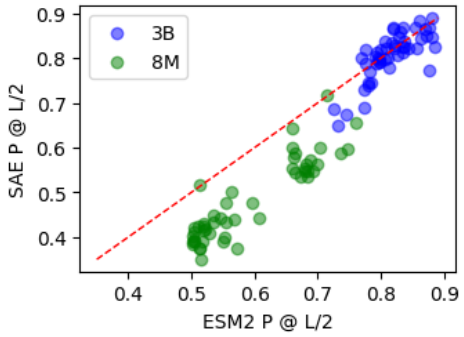


(b) Correlation plot on long-range contact accuracy measured by Precision at L/2 (P @ L/2) between ESM2 and SAE reconstructions on 8M and 3B subject model sizes.

Figure 3: Analysis of feature-concept relationships and long-range contact accuracy.

steering methodology of Templeton et al. (2024) and detailed in Appendix Section F, we steer this feature ($\alpha$ = -0.275) and observe significant changes in predicted protein surface accessibility of myoglobin (PDB ID: 1MBN) while maintaining structural integrity (Figure 4a).

Steering increased total Solvent Accessible Surface Area (SASA) by 31.5% (from 8,369.5 to 11,009.3 Å$^2$) with minimal structural disruption (RMSD 2.76 Å) in the expected range of Figure 2b. Feature intervention affected both sequence-level predictions via steering toward more hydrophilic residues and direct structural predictions of ESMFold (Figure 8). Critically, steering the hidden representation at layer 36 alone was sufficient to induce significant structural changes consistent with increased hydrophilicity, even when providing ESMFold with the correct input sequence (Figure 4b). Further details found in Appendix Section F.2 and feature validation in Appendix Section F.3.

## 6 Discussion

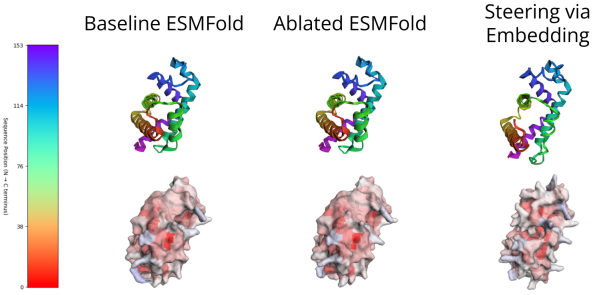


(a) Structural visualization of feature steering effect on myoglobin with $\alpha$= -0.275 on selected feature. Bottom row surface representation is colored by computed SASA, with blue as low, white as medium, and red as higher SASA.

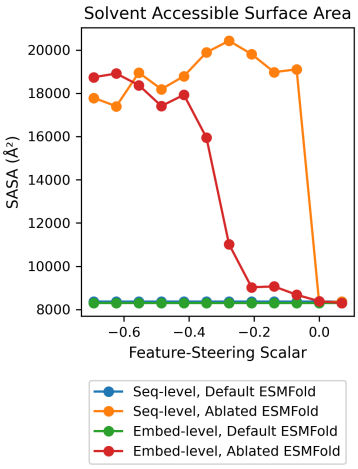


(b) Solvent accessible surface area (SASA) changes under different steering conditions.

Figure 4: Feature steering and SASA analysis.

This work advances PLM interpretability by scaling SAEs to ESM2-3B, extending recent work using SAEs to interpret PLMs to the structure prediction task (Simon and Zou (2024); Adams et al. (2025)). Through a combination of increasing subject model size, leveraging the Matryoshka architecture, and targeted interventions on ESMFold's structure predictions, we present the first work applying mechanistic interpretability to protein structure prediction.

### 6.1 Limitations

In the scope of this work, several limitations remain. First, although we take an important step toward mechanistic interpretability of protein structure prediction, our focus is exclusively on how PLM-derived sequence representations inform structure prediction. The interpretability of ESMFold's structure prediction head is left for future investigation. Second, our interventions on ESMFold were restricted to single-feature manipulations on embeddings from individual layers rather than exploring combinations of features or cross-layer interactions. Third, our analysis is limited to the 8M and 3B models of ESM2; evaluating a broader range of model sizes could reveal whether SAE performance eventually plateaus. Fourth, ESMFold is no longer state-of-the-art compared to newer diffusion-based protein structure prediction methods Abramson et al. (2024); Wohlwend et al. (2024); Watson et al. (2023).

Fifth, recent work suggests that SAEs can learn different features even when trained on the same data, implying that our results may be sensitive to both initialization and the specific UniRef50 sample used (Paulo and Belrose (2025)). Sixth, our structural steering experiments focused primarily on surface accessibility, leaving other potential structural properties unexplored, and the observed hydrophobicity effects might be achievable through simpler approaches such as steering smaller PLMs or using supervised linear probes. Seventh, for Matryoshka SAEs, we do not report how the number of groups and group size choices impact results. Finally, although our ablation studies demonstrate preservation of structural information, we have not fully characterized how interactions among SAE features might affect ESMFold's folding mechanism. We anticipate that future work leveraging our open-source models developed with substantial computational resources will address these limitations and yield further insights for the community.

### 6.2 Future Work

**Connections to Geometric Representations.** This work, while taking a significant step towards interpreting protein structure prediction, focuses primarily on learning linear representations of sequence information. Future work could establish formal connections between SAE sequence representations and equivariant representations of geometric data (Thomas et al., 2018; Geiger and Smidt, 2022; Lee et al., 2023), particularly investigating how the linear overcomplete basis learned by SAEs map to irreducible representations of geometric transformations in the context of protein structure prediction.

**Theoretical Analysis of Matryoshka SAEs.** Additionally, theoretical analysis drawing from ordered autoencoding (Rippel et al., 2014; Xu et al., 2021) and information bottleneck methods (Tishby et al., 2000) applied to protein structure prediction could improve our understanding of multi-scale feature learning in biological sequences. Such analysis may provide deeper insights into how hierarchical feature representations emerge and interact within the context of protein language models.

# 7 APPENDIX

## A MEANINGFULNESS STATEMENT

We consider meaningful biological representations to be those that enable humans to better understand and apply biological AI models in useful ways. Our work advances this goal by making the highly nonlinear representations in state-of-the-art protein structure prediction models more interpretable through sparse autoencoders, without sacrificing performance. By revealing the hierarchical organization of learned features and enabling targeted manipulation of structure predictions, our approach bridges the gap between black-box performance and biological understanding - a crucial step toward trustworthy and controllable protein design tools.

## B RELATED WORK

Recent work has focused on mechanistically interpreting protein language models (PLMs) to understand how they achieve remarkable success in protein modeling and design. Early interpretability studies examined PLM internals, with Vig et al. (2021) and Rao et al. (2021) discovering that attention patterns encode structural relationships between amino acids. Later work extended these findings, showing attention could identify functionally important regions like allosteric sites (Kannan et al. (2024); Dong et al. (2024)).

Building on this attention-based analysis, Zhang et al. (2024) provided key mechanistic insights by showing that PLMs primarily learn by storing and looking up coevolutionary patterns preserved through evolution, rather than learning fundamental protein physics. By analyzing what sequence features influence contact predictions through a "categorical Jacobian" method, they demonstrated that PLMs memorize statistics of co-evolving residues analogous to classic evolutionary models.

Sparse autoencoders (SAEs) have emerged as a powerful new tool for interpreting these models. Simon and Zou (2024) developed InterPLM, extracting thousands of interpretable features from ESM-2 that correspond to known biological concepts like binding sites, structural motifs, and functional domains. Their work revealed that most biological concepts exist in superposition within the model's neurons, as SAEs vastly outperformed individual neurons at capturing these concepts. Concurrently, Adams et al. (2025) explored different SAE training approaches and evaluated their biological relevance through novel downstream tasks. In this work, we scale SAE training and evaluation to ESM2-3B and introduce Matryoshka SAEs (Bussmann et al. (2024); Nabeshima (2024)) with hierarchical encoding to steer ESMFold's structure prediction capabilities for the first time.

## C SWISS-PROT EVALUATION

### C.1 BACKGROUND OF SWISS-PROT EVALUATION

Swiss-Prot is the gold standard manually curated section of the UniProt Knowledge Base, containing expert-annotated protein sequences with detailed information about their structure, function, modifications, and key biological regions (Poux et al. (2017); Consortium (2024)). Through extensive experimental validation and literature review, Swiss-Prot provides high-quality annotations that span from individual catalytic sites to complete functional domains. Following Simon and Zou (2024), we evaluate whether learned features align with these known biological concepts using a modified F1 score that handles the mismatch between precise feature activations and broader protein annotations present in Swiss-Prot. This approach calculates precision at the amino acid level but recall at the domain level, enabling systematic comparison between learned features and known biological concepts.

### C.2 PERFORMANCE OF SAE MODELS ON F1 CONCEPT EVALUATION

**Model Scale vs Architecture:** At 3B scale, architectural differences have minimal impact, with both Matryoshka and TopK identifying 233 concepts and showing only small variations in high-quality feature-concept pairs (2,677 vs 2,461). At 8M scale, architectural differences are more pronounced though still modest, with TopK outperforming Matryoshka (95 vs 72 concepts). However, the scale

effect dominates these architectural differences - both 3B variants substantially outperform both 8M variants across all concept types.

| Category | Total Concepts | Concepts with F1 $> 0.5$ (%) | | | |
|---|---|---|---|---|---|
| | | 3B MatK | 3B TopK | 8M MatK | 8M TopK |
| Domains | 256 | 193 (75.4%) | 195 (76.2%) | 50 (19.5%) | 72 (28.1%) |
| Regions | 55 | 19 (34.5%) | 20 (36.4%) | 10 (18.2%) | 13 (23.6%) |
| Motifs | 37 | 6 (16.2%) | 5 (13.5%) | 2 (5.4%) | 3 (8.1%) |
| Zinc Fingers | 15 | 5 (33.3%) | 5 (33.3%) | 2 (13.3%) | 2 (13.3%) |
| Other Features | 10 | 5 (50.0%) | 3 (30.0%) | 4 (40.0%) | 1 (10.0%) |
| Targeting Peptides | 5 | 5 (100.0%) | 5 (100.0%) | 4 (80.0%) | 4 (80.0%) |
| Total | 476 | 233 (48.9%) | 233 (48.9%) | 72 (15.1%) | 95 (20.0%) |

Table 1: Concept coverage comparison across model scales and architectures. We report the number (percentage) of concepts with F1 scores exceeding 0.5 for each model variant, broken down by concept category.

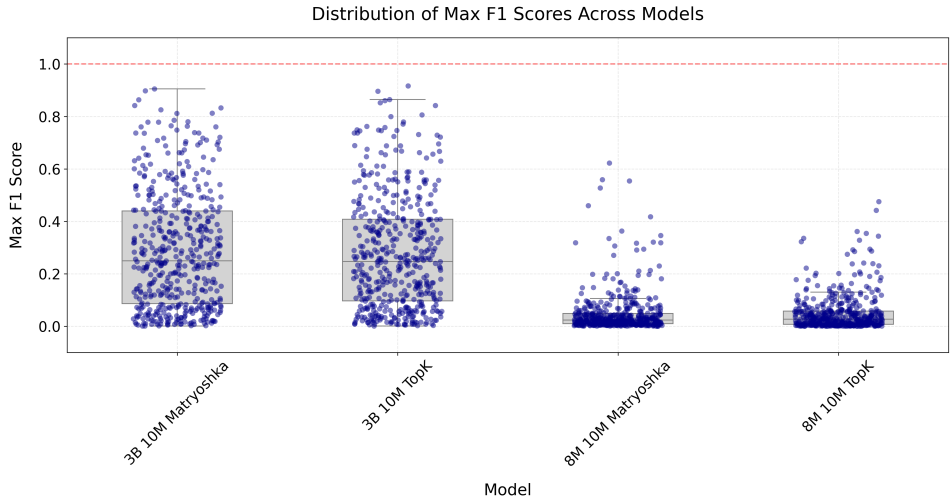


Figure 5: Distribution of highest F1 scores achieved for each concept across models.

The boxplot distribution reveals a clear separation between model scales (5. The 3B models show broader distributions with medians around 0.4 and numerous concepts achieving scores above 0.6. In contrast, 8M models show compressed distributions with medians below 0.1, indicating substantially weaker concept capture across the board.

The comparison heatmaps demonstrate relative performance between model variants by comparing their best-performing features for each concept. The left heatmap shows the number of concepts where each row model achieves a higher F1 score than the column model, while the right heatmap shows the average F1 score difference (Figure 6). The 3B models outperform 8M variants on approximately 400 concepts, with an average F1 improvement of 0.25. Within each scale, architectural variants show minimal differences (average F1 difference $< 0.01$), suggesting model scale rather than architecture drives concept capture ability.

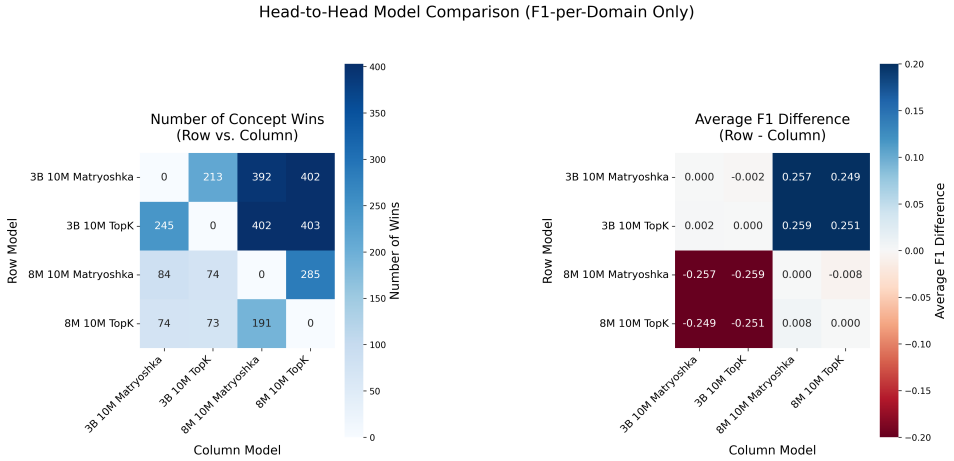


Figure 6: Left: Number of concepts where the row model achieves a higher maximum F1 score for a given concept than the column model. Right: Average score difference of the highest F1 scores for a given concept between models (row minus column) across all concepts. Each cell compares the best-performing feature for each concept between model pairs. Darker blue indicates stronger performance advantage for the row model.

## D CASP14 Dataset

We downloaded the CASP14 targets dataset from the CASP14 website here.

After filtering, we benchmark on these targets: [T1024, T1025, T1026, T1029, T1030, T1032, T1046s1, T1046s2, T1050, T1054, T1056, T1067, T1073, T1074, T1079, T1082, T1090].

## E Contact Map Prediction

**Motivation.** Zhang et al. (2024) introduced the Categorical Jacobian calculation to extract coevolutionary signals from protein language models in an unsupervised manner via masked language modeling. Given that SAEs also learn through unsupervised training, we adapt this approach for contact map prediction to evaluate whether SAEs preserve coevolutionary patterns and structural information learned by ESM2.

**Data.** We subset the evaluation dataset to the top 50 proteins ranked by precision at $L/2$ on ESM2-3B due to computational constraints. This subset was used as a positive control, and we did not have time to rerun the full analysis before the submission deadline. We acknowledge that this approach introduces a bias favoring the claim that ESM2-3B outperforms 8M, which will be addressed in a subsequent revision. Nonetheless, we expect the claim to remain valid, as ESM2-3B significantly outperforms 8M across nearly the entire dataset of Zhang et al. (2024), as illustrated in Fig. 7.

**Hyperparameters.** In Fig 3b, our SAEs were trained on layer 36 with TopK architecture with expansion factors 16x for ESM2-8M (dict size 10240) and 8x for ESM2-3B (dict size 20480). We did not rerun for the Matryoshka architecture given TopK's similar language modeling reconstruction performance and how computationally expensive it is.

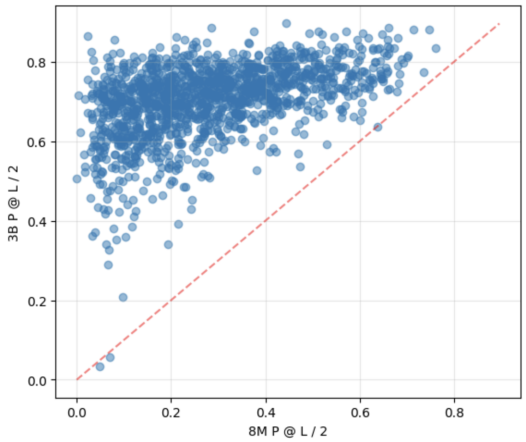


Figure 7: Contact Map Accuracy for Cat. Jacobian on ESM2 8M vs 3B, N=1412/1431

# F ESMFold Steering Case Study

## F.1 Feature Steering Background

Following the method described in Templeton et al. (2024), each target feature is represented by its corresponding decoder vector ($d_{(i)} = W_{dec}[i, :]$), which is normalized to unit norm during training, and an intervention is performed by adding a scaled version of this vector to the hidden state ($h_l \leftarrow h_l + \alpha \cdot d_{(i)}$) to amplify or suppress that feature's contribution. In our approach, we apply a maximum activation scaling factor during training and subsequently scale the encoder and decoder biases at inference. This means our effective steering coefficient, reported in all figures and results, is given by $\alpha' = \text{norm\_factor} \cdot \alpha$, ensuring consistent steering effects across different model configurations.

## F.2 Details of Feature Steering Case Study

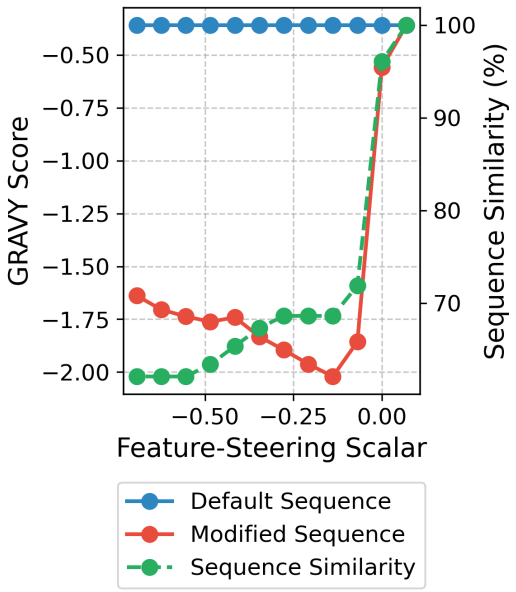


Figure 8: Plot of sequence GRAVY scores overlaid with sequence similarity with increased feature steering

Our intervention framework employed two complementary approaches: (1) examining sequence-level changes through standard ESMFold predictions, and (2) directly intervening on hidden representations while maintaining the true input sequence in an ablated version that isolated intervention effects. This design allowed us to dissect how structural information flows through the model. The ablated model showed minimal performance differences (Figure 2b).

The feature (f/2) was identified in the first group of a Matryoshka SAE trained on hidden layer 36 (dictionary size 10,240, group fractions [0.002, 0.0156, 0.125, 0.8574], sparsity k=20), showing strong correlation with residue hydrophobicity. We selected the Matryoshka SAE architecture as its hierarchical encoding tends to capture broader concepts in earlier groups, which we hypothesized would enable more robust steering across diverse proteins. We applied the steering methodology from Templeton et al. (2024), adding the decoder vector with coefficient $\alpha$ = -0.275. SASA was computed using FreeSASA Mitternacht (2016) with default parameters. The observed RMSD of 2.76 Å aligns with typical deviations for ESMFold with layer 36 LM head ablation, while ablating other ESM2 layer representations resulted in RMSD of 0.191 compared to regular ESMFold (Figure 2b).

As shown in Figure 8, steering progressively decreased sequence GRAVY scores, indicating a shift toward hydrophilic residues. When modified sequences were processed through default ESMFold, we observed even larger SASA increases, consistent with replacing hydrophobic core residues with hydrophilic ones. This effect manifested through two distinct mechanisms: direct biasing of the structure module toward more exposed conformations (even with correct sequence information), and shifting sequence predictions toward more hydrophilic residues when allowed to influence the sequence module. Notably, structural changes persisted even when preserving the original sequence, suggesting ESMFold's predictions are influenced by hidden representations corresponding to the modified sequence despite having access to correct sequence information.

### F.3 Validation of Case Study Feature Steering Directionality and Specificity

| Scalar | Modified SASA | SASA Change | Modified GRAVY | GRAVY Change |
|---|---|---|---|---|
| 0.069 | 8369.55 | 0.00% | -0.3588 | 0.00% |
| 0.208 | 8351.58 | -0.21% | -0.0595 | +83.42% |
| 0.346 | 8568.43 | +2.38% | 0.6569 | +283.08% |
| 0.554 | 8616.49 | +2.95% | 1.3046 | +463.60% |
| 0.693 | 9719.28 | +16.13% | 1.5255 | +525.17% |

Table 2: Positive steering control results showing changes in SASA and GRAVY scores relative to baseline values.

| Feature | Metric | Scalar Values | | |
|---|---|---|---|---|
| | | -0.069 | -0.346 | -0.693 |
| Feature 5 (Group 1) | $\delta$SASA | 0.00% | +0.38% | -0.54% |
| | $\delta$GRAVY | 0.00% | +40.40% | +52.34% |
| Feature 39 (Group 2) | $\delta$SASA | 0.00% | 0.00% | 0.00% |
| Feature 1381 (Group 3) | $\delta$SASA | 0.00% | 0.00% | 0.00% |
| Feature 7921 (Group 4) | $\delta$SASA | 0.00% | 0.00% | 0.00% |
| | $\delta$GRAVY | 0.00% | 0.00% | 0.00% |
| Original Experiment | $\delta$SASA | +128.44% | +137.12% | +112.89% |
| | $\delta$GRAVY | -417.34% | -446.21% | -356.69% |

Table 3: Comparison of random feature controls with original experiment, showing percentage changes relative to unsteered (scalar=0) values.

We performed positive steering control experiments to validate the directional behavior of our feature, applying scalar values from 0.069 to 0.693. As predicted, steering the feature positively resulted

in a systematic increase in hydrophobicity (GRAVY score) while maintaining structural stability at moderate steering strengths. The modified sequence GRAVY scores increased from -0.36 to 1.53, reflecting enhanced hydrophobic content, while SASA values remained stable ($\leq 3\%$ change) until the highest scalar values where minor structural perturbations emerged.

Additionally, to assess the specificity of identified feature, we performed negative steering experiments on randomly selected features from each Matryoshka group (features 5, 39, 1381, and 7921). Unlike our target feature, random features showed minimal response to steering, with three features showing no changes ($\leq 0.1\%$ variation) across all metrics and one feature (Feature 5) showing only minor variations incomparable to the dramatic shifts observed in our main experiment.

# G Implementation Details

## G.1 Code

For all SAE implementations, we use Marks et al. (2024). For our L1 regularized SAEs, we follow Conerly et al. (2024). For TopK, we follow Gao et al. (2024). In Fig 2a, we standardize hyperparameters with an expansion factor of 8x (dict size 20480) and batch size 2048 and use best learning rate.

## G.2 Data Curation

Following the approach outlined in the InterPLM paper, we first process the UniRef50 FASTA file by iterating over each protein sequence. We remove any sequence that exceeds 1022 tokens, as ESM-2 cannot process longer inputs. From the remaining sequences, we randomly select a predetermined number of proteins to create our working dataset. This dataset is then divided into shards of 1000 sequences each, facilitating efficient handling during training.

## G.3 Optimizing the Dataset and Training Procedure

After generating embeddings with ESM-2, the activations are stored as tensors representing entire shards. We then use Litdata's optimize function to iterate through each tensor and split it into fixed-size batches. The optimized dataset achieves speedup by reducing streaming I/O overhead to AWS S3 during training. Additionally, the optimized dataset uses Litdata's StreamingDataset and StreamingDataloader where we shuffle the batches during training, while also leveraging PyTorch Lightning for multi-GPU training support.

## REFERENCES

John Jumper, Richard Evans, Alexander Pritzel, Tim Green, Michael Figurnov, Olaf Ronneberger, Kathryn Tunyasuvunakool, Russ Bates, Augustin Žídek, Anna Potapenko, Alex Bridgland, Clemens Meyer, Simon A. A. Kohl, Andrew J. Ballard, Andrew Cowie, Bernardino Romera-Paredes, Stanislav Nikolov, Rishub Jain, Jonas Adler, Trevor Back, Stig Petersen, David Reiman, Ellen Clancy, Michal Zielinski, Martin Steinegger, Michalina Pacholska, Tamas Berghammer, Sebastian Bodenstein, David Silver, Oriol Vinyals, Andrew W. Senior, Koray Kavukcuoglu, Pushmeet Kohli, and Demis Hassabis. Highly accurate protein structure prediction with alphafold. *Nature*, 596(7873):583–589, August 2021. ISSN 1476-4687. doi: 10.1038/s41586-021-03819-2. URL https://doi.org/10.1038/s41586-021-03819-2.

Zeming Lin, Halil Akin, Roshan Rao, Brian Hie, Zhongkai Zhu, Wenting Lu, Nikita Smetanin, Robert Verkuil, Ori Kabeli, Yaniv Shmueli, Allan dos Santos Costa, Maryam Fazel-Zarandi, Tom Sercu, Salvatore Candido, and Alexander Rives. Evolutionary-scale prediction of atomic level protein structure with a language model. *bioRxiv*, 2022. doi: 10.1101/2022.07.20.500902. URL https://www.biorxiv.org/content/early/2022/12/21/2022.07.20.500902.

Debora S. Marks, Lucy J. Colwell, Robert Sheridan, Thomas A. Hopf, Andrea Pagnani, Riccardo Zecchina, and Chris Sander. Protein 3d structure computed from evolutionary sequence variation. *PLOS ONE*, 6(12):1–20, 12 2011. doi: 10.1371/journal.pone.0028766. URL https://doi.org/10.1371/journal.pone.0028766.

Hetunandan Kamisetty, Sergey Ovchinnikov, and David Baker. Assessing the utility of coevolution-based residue–residue contact predictions in a sequence- and structure-rich era. *Proceedings of the National Academy of Sciences*, 110(39):15674–15679, 2013. doi: 10.1073/pnas.1314045110. URL https://www.pnas.org/doi/abs/10.1073/pnas.1314045110.

Roshan Rao, Joshua Meier, Tom Sercu, Sergey Ovchinnikov, and Alexander Rives. Transformer protein language models are unsupervised structure learners. In *International Conference on Learning Representations*, 2021. URL https://openreview.net/forum?id=fylclEqgvgd.

Jesse Vig, Ali Madani, Lav R. Varshney, Caiming Xiong, Richard Socher, and Nazneen Fatema Rajani. Bertology meets biology: Interpreting attention in protein language models, 2021. URL https://arxiv.org/abs/2006.15222.

Zhidian Zhang, Hannah K. Wayment-Steele, Garyk Brixi, Haobo Wang, Dorothee Kern, and Sergey Ovchinnikov. Protein language models learn evolutionary statistics of interacting sequence motifs. *Proceedings of the National Academy of Sciences*, 121(45):e2406285121, 2024. doi: 10.1073/pnas.2406285121. URL https://www.pnas.org/doi/abs/10.1073/pnas.2406285121.

Adly Templeton, Tom Conerly, Jonathan Marcus, Jack Lindsey, Trenton Bricken, Brian Chen, Adam Pearce, Craig Citro, Emmanuel Ameisen, Andy Jones, Hoagy Cunningham, Nicholas L Turner, Callum McDougall, Monte MacDiarmid, C. Daniel Freeman, Theodore R. Sumers, Edward Rees, Joshua Batson, Adam Jermyn, Shan Carter, Chris Olah, and Tom Henighan. Scaling monosemanticity: Extracting interpretable features from claude 3 sonnet. *Transformer Circuits Thread*, 2024. URL https://transformer-circuits.pub/2024/scaling-monosemanticity/index.html.

Leo Gao, Tom Dupré la Tour, Henk Tillman, Gabriel Goh, Rajan Troll, Alec Radford, Ilya Sutskever, Jan Leike, and Jeffrey Wu. Scaling and evaluating sparse autoencoders, 2024. URL https://arxiv.org/abs/2406.04093.

Elana Simon and James Zou. Interplm: Discovering interpretable features in protein language models via sparse autoencoders. *bioRxiv*, 2024. doi: 10.1101/2024.11.14.623630. URL https://www.biorxiv.org/content/early/2025/01/28/2024.11.14.623630.

Etowah Adams, Liam Bai, Minji Lee, Yiyang Yu, and Mohammed AlQuraishi. From mechanistic interpretability to mechanistic biology: Training, evaluating, and interpreting sparse autoencoders

on protein language models. *bioRxiv*, 2025. doi: 10.1101/2025.02.06.636901. URL https://www.biorxiv.org/content/early/2025/02/08/2025.02.06.636901.

Noa Nabeshima. Matryoshka sparse autoencoders, December 2024. URL https://www.lesswrong.com/posts/zbebxYCqsryPALh8C/matryoshka-sparse-autoencoders. AI Alignment Forum, Accessed: Feb 10, 2025.

Bart Bussmann, Patrick Leask, and Neel Nanda. Learning multi-level features with matryoshka saes, December 2024. URL https://www.lesswrong.com/posts/rKM9b6B2LqwSB5ToN/learning-multi-level-features-with-matryoshka-saes#What_are_Matryoshka_SAEs__. AI Alignment Forum, Accessed: Feb 10, 2025.

Samuel Marks, Adam Karvonen, and Aaron Mueller. dictionary_learning package. https://github.com/saprmarks/dictionary_learning, 2024.

Ian Sillitoe, Nicola Bordin, Natalie Dawson, Vaishali P Waman, Paul Ashford, Harry M Scholes, Camilla S M Pang, Laurel Woodridge, Clemens Rauer, Neeladri Sen, Mahnaz Abbasian, Sean Le Cornu, Su Datt Lam, Karel Berka, Ivana Hutařová Varekova, Radka Svobodova, Jon Lees, and Christine A Orengo. Cath: increased structural coverage of functional space. *Nucleic Acids Research*, 49(D1):D266–D273, 11 2020. ISSN 0305-1048. doi: 10.1093/nar/gkaa1079. URL https://doi.org/10.1093/nar/gkaa1079.

Josh Abramson, Jonas Adler, Jack Dunger, Richard Evans, Tim Green, Alexander Pritzel, Olaf Ronneberger, Lindsay Willmore, Andrew J. Ballard, Joshua Bambrick, Sebastian W. Bodenstein, David A. Evans, Chia-Chun Hung, Michael O'Neill, David Reiman, Kathryn Tunyasuvunakool, Zachary Wu, Akvilė Žemgulytė, Eirini Arvaniti, Charles Beattie, Ottavia Bertolli, Alex Bridgland, Alexey Cherepanov, Miles Congreve, Alexander I. Cowen-Rivers, Andrew Cowie, Michael Figurnov, Fabian B. Fuchs, Hannah Gladman, Rishub Jain, Yousuf A. Khan, Caroline M. R. Low, Kuba Perlin, Anna Potapenko, Pascal Savy, Sukhdeep Singh, Adrian Stecula, Ashok Thillaisundaram, Catherine Tong, Sergei Yakneen, Ellen D. Zhong, Michal Zielinski, Augustin Žídek, Victor Bapst, Pushmeet Kohli, Max Jaderberg, Demis Hassabis, and John M. Jumper. Accurate structure prediction of biomolecular interactions with alphafold 3. *Nature*, 630(8016):493–500, June 2024. ISSN 1476-4687. doi: 10.1038/s41586-024-07487-w. URL https://doi.org/10.1038/s41586-024-07487-w.

Jeremy Wohlwend, Gabriele Corso, Saro Passaro, Mateo Reveiz, Ken Leidal, Wojtek Swiderski, Tally Portnoi, Itamar Chinn, Jacob Silterra, Tommi Jaakkola, and Regina Barzilay. Boltz-1: Democratizing biomolecular interaction modeling. *bioRxiv*, 2024. doi: 10.1101/2024.11.19.624167. URL https://www.biorxiv.org/content/early/2024/12/27/2024.11.19.624167.

Joseph L. Watson, David Juergens, Nathaniel R. Bennett, Brian L. Trippe, Jason Yim, Helen E. Eisenach, Woody Ahern, Andrew J. Borst, Robert J. Ragotte, Lukas F. Milles, Basile I. M. Wicky, Nikita Hanikel, Samuel J. Pellock, Alexis Courbet, William Sheffler, Jue Wang, Preetham Venkatesh, Isaac Sappington, Susana Vázquez Torres, Anna Lauko, Valentin De Bortoli, Emile Mathieu, Sergey Ovchinnikov, Regina Barzilay, Tommi S. Jaakkola, Frank DiMaio, Minkyung Baek, and David Baker. De novo design of protein structure and function with rfdiffusion. *Nature*, 620(7976):1089–1100, August 2023. ISSN 1476-4687. doi: 10.1038/s41586-023-06415-8. URL https://doi.org/10.1038/s41586-023-06415-8.

Gonçalo Paulo and Nora Belrose. Sparse autoencoders trained on the same data learn different features, 2025. URL https://arxiv.org/abs/2501.16615.

Nathaniel Thomas, Tess E. Smidt, Steven Kearnes, Lusann Yang, Li Li, Kai Kohlhoff, and Patrick Riley. Tensor field networks: Rotation- and translation-equivariant neural networks for 3d point clouds. *CoRR*, abs/1802.08219, 2018. URL http://arxiv.org/abs/1802.08219.

Mario Geiger and Tess Smidt. e3nn: Euclidean neural networks, 2022. URL https://arxiv.org/abs/2207.09453.

Jae Hyeon Lee, Payman Yadollahpour, Andrew Watkins, Nathan C. Frey, Andrew Leaver-Fay, Stephen Ra, Kyunghyun Cho, Vladimir Gligorijević, Aviv Regev, and Richard Bonneau. Equifold: Protein structure prediction with a novel coarse-grained structure representation. *bioRxiv*, 2023. doi: 10.1101/2022.10.07.511322. URL https://www.biorxiv.org/content/early/2023/01/02/2022.10.07.511322.

Oren Rippel, Michael A. Gelbart, and Ryan P. Adams. Learning ordered representations with nested dropout, 2014. URL https://arxiv.org/abs/1402.0915.

Yilun Xu, Yang Song, Sahaj Garg, Linyuan Gong, Rui Shu, Aditya Grover, and Stefano Ermon. Anytime sampling for autoregressive models via ordered autoencoding. *CoRR*, abs/2102.11495, 2021. URL https://arxiv.org/abs/2102.11495.

Naftali Tishby, Fernando C. Pereira, and William Bialek. The information bottleneck method, 2000. URL https://arxiv.org/abs/physics/0004057.

Gokul R. Kannan, Brian L. Hie, and Peter S. Kim. Single-sequence, structure free allosteric residue prediction with protein language models. *bioRxiv*, 2024. doi: 10.1101/2024.10.03.616547. URL https://www.biorxiv.org/content/early/2024/10/03/2024.10.03.616547.

Tianze Dong, Christopher Kan, Kapil Devkota, and Rohit Singh. Allo-allo: Data-efficient prediction of allosteric sites. *bioRxiv*, 2024. doi: 10.1101/2024.09.28.615583. URL https://www.biorxiv.org/content/early/2024/09/30/2024.09.28.615583.

Sylvain Poux, Cecilia N Arighi, Michele Magrane, Alex Bateman, Chih-Hsuan Wei, Zhiyong Lu, Emmanuel Boutet, Hema Bye-A-Jee, Maria Livia Famiglietti, Bernd Roechert, and The UniProt Consortium. On expert curation and scalability: Uniprotkb/swiss-prot as a case study. *Bioinformatics*, 33(21):3454–3460, 07 2017. ISSN 1367-4803. doi: 10.1093/bioinformatics/btx439. URL https://doi.org/10.1093/bioinformatics/btx439.

The UniProt Consortium. Uniprot: the universal protein knowledgebase in 2025. *Nucleic Acids Research*, 53(D1):D609–D617, 11 2024. ISSN 1362-4962. doi: 10.1093/nar/gkae1010. URL https://doi.org/10.1093/nar/gkae1010.

Simon Mitternacht. Freesasa: An open source c library for solvent accessible surface area calculations. *F1000Research*, 5:189, February 2016. ISSN 2046-1402. doi: 10.12688/f1000research.7931.1. URL http://dx.doi.org/10.12688/f1000research.7931.1.

Tom Conerly, Adly Templeton, Trenton Bricken, Jonathan Marcus, and Tom Henighan. April 2024 update on transformer circuits. *Transformer Circuits*, 2024. URL https://transformer-circuits.pub/2024/april-update/index.html.